Published in final edited form as:

J Comp Neurol. 2019 January 01; 527(1): 297–311. doi:10.1002/cne.24556.

The M6 cell: A small-field bistratified photosensitive retinal ganglion cell

Lauren E. Quattrochi[1], **Maureen E. Stabio**[2], **Inkyu Kim**[1], **Marissa C. Ilardi**[1], **P. Michelle Fogerson**[1], **Megan L. Leyrer**[1], and **David M. Berson**[1]

[1]Department of Neuroscience and Carney Institute for Brain Science, Brown University, Providence, RI 02912, USA

[2]Department of Cell & Developmental Biology, University of Colorado School of Medicine, Aurora, CO 80018, USA

Abstract

We have identified a novel, sixth type of intrinsically photosensitive retinal ganglion cell (ipRGC) in the mouse — the M6 cell. Its spiny, highly branched dendritic arbor is bistratified, with dendrites restricted to the inner and outer margins of the inner plexiform layer, co-stratifying with the processes of other ipRGC types. We show that M6 cells are by far the most abundant ganglion cell type labeled in adult pigmented Cdh3-GFP BAC transgenic mice. A few M5 ipRGCs are also labeled, but no other RGC types were encountered. Several distinct subnuclei in the geniculate complex and the pretectum contain labeled retinofugal axons in the Cdh3-GFP mouse. These are presumably the principle central targets of M6 cells (as well as M4 and M5 cells). Projections from M6 cells to the dorsal lateral geniculate nucleus were confirmed by retrograde tracing, suggesting they contribute to pattern vision. M6 cells have low levels of melanopsin expression and relatively weak melanopsin-dependent light responses. They also exhibit strong synaptically driven light responses. Their dendritic fields are the smallest and most abundantly branched of all ipRGCs. They have small receptive fields and strong antagonistic surrounds. Despite deploying dendrites partly in the OFF sublamina, M6 cells appear to be driven exclusively by the ON pathway, suggesting that their OFF arbor, like those of certain other ipRGCs, may receive ectopic input from passing ON bipolar cells axons in the OFF sublayer.

Graphical Abstract

Correspondence to: David_Berson@brown.edu, Box G-LN, Brown University, Providence, RI 02912.

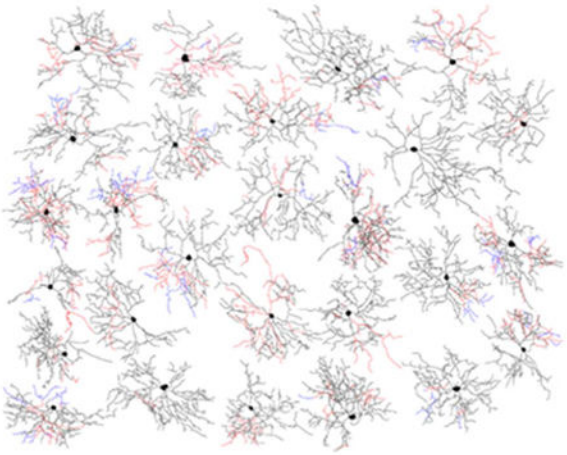

Welcome the sixth member of the family of photosensitive retinal ganglion cells (ipRGCs) discovered in the mouse retina, named the M6 cell. This cell is morphologically unique among ipRGCs by its small diameter, highly branched, spiny, bi-stratified dendritic arbor (ON-black; OFF-red), with frequent appearance of recursive 'diving' dendrites (blue).

Keywords

cadherin; ganglion cell photoreceptors; intrinsically photosensitive retinal ganglion cells; lateral geniculate nucleus; melanopsin; retinal ganglion cells; RRID: AB_2079751; RRID: AB_11214110; RRID: AB_1608077; RRID: AB_221570; RRID: AB_2536190; RRID: AB_2534105; RRID: AB_142540; RRID: AB_141844; RRID: AB_2535792; RRID: AB_141637; RRID: AB_143165; RRID: AB_141359; RRID: AB_141930; RRID: AB_2716806

Introduction

Melanopsin-expressing intrinsically photosensitive retinal ganglion cells (ipRGCs) are diverse. In mice, they comprise five distinct types, M1 through M5 (Schmidt, Chen, & Hattar, 2011; Sonoda & Schmidt, 2016; Stabio et al., 2018). Each has a characteristic pattern of melanopsin expression, soma-dendritic morphology and brain projections. The present study was motivated by clues that at least one additional ipRGC type might remain to be identified. In our earlier survey in a melanopsin reporter mouse (Ecker et al., 2010), a few labeled cells were intrinsically photosensitive, yet had highly branched, spiny dendritic arbors apparently distinct from those of the known ipRGC types. A second clue came from transgenic mice designed to label cells expressing cadherin-3 with green fluorescent protein (GFP; Cdh3-GFP mice (Osterhout, El-Danaf, Nguyen, & Huberman, 2014; Osterhout et al., 2011). In these mice, a small fraction of RGCs express GFP, and their axons terminate almost exclusively in known targets of ipRGCs, such as the olivary pretectal nucleus (OPN) and the ventral lateral geniculate nucleus (vLGN), yet they lacked detectable melanopsin immunoreactivity. Their morphology was reminiscent of the spiny cells we had occasionally encountered in the melanopsin reporter mouse, so we suspected they might be true ipRGCs, even though they express levels of melanopsin too low to be detected immunohistochemically (see (Estevez et al., 2012; Stabio et al., 2018). Alternatively, they

could represent a new type of conventional RGCs with outputs that converge with those of ipRGCs in a subset of ‘non-image-forming’ targets.

Osterhout et al. (2011, 2014) reported that two highly branched ganglion cell types accounted for most of the GFP-labeled cells in the Cdh3-GFP mouse: Type 1 cells, whose dendritic arbors are monostratified within the ON sublayer of the inner plexiform layer (IPL); and Type 2 cells, which are bistratified, with separate ON and OFF arbors. They also reported that a small fraction (<10%) of Cdh3-GFP cells were melanopsin immunopositive by conventional immunohistochemistry (without amplification methods), but did not determine whether these corresponded to Type 1 (monostratified) or Type 2 (bistratified) Cdh3-GFP cells or to a previously characterized ipRGC type.

Here, we demonstrate that the bistratified Cdh3-GFP cells are indeed intrinsically photosensitive. We call them “M6 cells,” extending the prevailing nomenclature for ipRGC types. We find that M6 cells express low levels of melanopsin and have correspondingly weak intrinsic light responses. They have ON-dominant synaptically driven light responses, and relatively small receptive fields with strong surrounds. We also show that the other major fluorescent ganglion-cell type in the Cdh3-GFP cell, the monostratified previously termed Type 1, is also intrinsically photosensitive and apparently corresponds to the M5 ipRGC type. We never encountered M1, M2, M3 or M4 cells among the fluorescent cells in the adult Cdh3-GFP mouse. Thus, the restricted brain projections labeled in this mouse (OPN, IGL, vLGN and weakly to dLGN) can be viewed as deriving mainly from M6 ipRGCs, with a smaller contribution from M5 cells.

Methods

Animals

All experiments were conducted in accordance with NIH guidelines under protocols approved by the Institutional Animal Care and Use Committee of Brown University. Two genetic strains of mice were used. The first, Cdh3-GFP, was derived from a transgenic mouse line generated by the GENSAT project. A transgene delivered through a bacterial artificial chromosome (BAC) drove the expression of GFP under the control of the promoter for cadherin-3. This strain, originally obtained from the MMRRC under the strain name Tg(Cdh3-EGFP)BK102Gsat/Mmnc, has been used in two earlier reports (Osterhout et al., 2014; Osterhout et al., 2011). The albino (Swiss Webster) background on which these mice were originally generated, is unsuitable for retinal physiology, so we back-crossed these mice to the C57BL6/J strain for several generations in order to obtain pigmented mice carrying the transgene. Both male and female mice were used and, unless otherwise stated, these ranged in age from postnatal days 25 to 43 (P25-43). The second strain, Opn4$^{cre/+}$;Z/EG$^{+/-}$ mice, were obtained by crossing homozygous Opn4$^{cre/cre}$ mice, in which *cre* was knocked into the melanopsin locus (Ecker et al., 2010), with mice heterozygous for the Z/EG transgene, a lox-stop-lox allele that drives expression of enhanced GFP selectively in Cre-expressing cells (Novak, Guo, Yang, Nagy, & Lobe, 2000). These mice, which were on a mixed genetic background, have been used in several prior studies of ipRGCs (Ecker et al., 2010; Estevez et al., 2012; Hu, Hill, & Wong, 2013; Stabio et al., 2018). We used Opn4$^{cre/+}$;Z/EG$^{+/-}$ mice of both sexes and ranging from 6 weeks to 4 months old.

Tissue Preparations and Solutions

Mice were sacrificed by inhalation of CO_2; all subsequent eye dissection procedures were performed under dim red light. Prior to removing the eye, the dorsal margin of the cornea was marked with a cautery. This was used to guide the placement of a large relieving cut in the dorsal retina as a subsequent guide to retinal orientation. Retinas were dissected free from the globe and vitreous removed while submerged in Ames' medium (Sigma) supplemented with 23mM $NaHCO_3$ and 10nM D-glucose and bubbled with 95% O_2/5% CO_2 at ambient temperature. The entire retina was mounted ganglion-side up in a glass chamber, secured in place with a slice anchor (Warner Instruments), and bathed in the same Ames' solution at a flow rate of 4mL/min, maintained at 30-33 °C with a feedback-controlled in-line heater (ATR-4, Quest Scientific or TC-324B, Warner Instruments). For voltage-clamp recordings, the internal pipette solution contained (in mM) 120 Cs-methanesulfonate, 5 NaCl, 4 CsCl, 2 EGTA, 10 HEPES, 4 ATP-Mg, 7 phosphocreatine-Tris, 0.3 GTP-Tris and 2 QX-314 (Estevez et al., 2012). For current-clamp recordings, Cs-methanesulfonate and CsCl were replaced with equimolar K-gluconate and KCl, respectively; in addition, the QX-314 was omitted. Intracellular solutions were adjusted to pH 7.4 with NaOH for voltage clamp and KOH for current clamp, and ranged in osmolarity from 270-280mOsm. Lucifer yellow or Alexa488 hydrazide were included in the internal solution for dye filling and morphological analysis of recorded cells (Estevez et al., 2012). To test for intrinsic photosensitivity, synaptic transmission was blocked by bath application of a drug cocktail containing 100 μm L-(+)-2-amino-4-phosphonobutyric acid (L-AP4), 40 μm 6,7-dinitroquinoxaline-2,3-dione (DNQX) and 30 μm D-(−)-2-amino-5-phosphonopentanoic acid (D-AP5), as previously detailed (Estevez et al., 2012; Wong, Dunn, & Berson, 2005; Wong, Dunn, Graham, & Berson, 2007).

Binocular Enucleation

Binocular enucleation was performed in P5 Cdh3-GFP mice. Animals were maintained on a warm heating pad throughout surgery and recovery. Animals were anesthetized with ketamine (100 mg/kg) and dexdormitor (0.5 mg/kg) and were given Buprenorphine SR for analgesia (1 mg/kg SC). Eyelids were gently opened with a scalpel blade and retracted with forceps to expose the eye. Eyes were removed by making a small incision to deflate the eye followed by removal with forceps and scissors. Gelfoam was placed in the sockets until bleeding subsided. Animals were given antisedan (0.1 mL per 10 g of mouse of a 0.025 mg/mL drug solution) to speed recovery from anesthesia. Animals were sacrificed 18 days after surgery to ensure near complete degeneration of optic axons. Animals were perfused with 4% PFA prior to brain removal.

Retrograde tracing

Retrograde tracer injections were performed as previously described (Estevez et al., 2012; Stabio et al., 2018). $Opn4^{cre/+}$;$Z/EG^{+/-}$ mice were anesthetized by inhalation of 3% isoflurane and placed in a stereotaxic apparatus. To label RGCs projecting to the dLGN, injections were conducted using either the retrograde tracing dye cholera toxin subunit β, alexa 594 conjugate (Invitrogen) or rhodamine latex microspheres (Lumafluor). Tracer (~200nL) was injected into the dLGN through a glass micropipette via pneumatic pressure

pulses (Picospritzer II, Parker Hannifin). Mice were euthanized one or more days after injection, and contralateral retinas were isolated for histology. Morphology of retrolabeled ipRGCs were identified either by ocular injection of a cre-dependent virus performed 2-4 weeks prior to retrograde tracing or intracellular dye filling immediately after retinal extraction (both described below).

Ocular injections

Opn4$^{cre/+}$;Z/EG$^{+/-}$ mice were anesthetized with isoflurane (3% in O_2). Eyes were gently exposed using forceps, and a glass pipette tip was inserted into the corneal-scleral border. 1.5-2 μL of cre-dependent virus (AAV2-CAG-flex-GFP; UNC Vector Core) was injected into the vitreous humor using pneumatic pressure pulses. Retrograde tracer was injected into the contralateral dLGN 2-4 weeks after ocular injection to ensure sufficient viral labeling prior to morphological analysis.

Intracellular dye injections

EGFP-labeled RGCs in whole-mount retinas from Cdh3-GFP and Opn4$^{cre/+}$;Z/EG$^{+/-}$ lines were targeted using sharp micropipettes containing Alexa-488 or Lucifer yellow. Dye was ejected via iontophoretic current as detailed by Pu and colleagues (Pu, Berson, & Pan, 1994). Only brightly, completely filled cells were included in the morphological analysis.

Whole-cell physiology

Whole-cell patch-clamp recordings were performed with a Multiclamp 700A amplifier coupled to a Digidata 1322 digitizer with pClamp9.2 data acquisition software (Molecular Devices). Mercury epifluorescence imaging (460 – 500 nm) was used to select a GFP+ ganglion cell for recording (Estevez et al., 2012; Van Hook, Wong, & Berson, 2012). Exposure to the mercury beam was kept as brief as possible, and at least 20 min passed after this exposure before light responses were tested. Thus, the retinas, although recorded in darkness, were in a bleach-adapted state during all subsequent recordings as described previously (Estevez et al., 2012). Under infrared illumination, a micropipette was used to tear a small hole in the inner limiting membrane overlying the ganglion cell of interest. Whole-cell recordings were made with patch pipettes pulled on a Flaming/Brown P-97 puller (Sutter Instruments). Resistances ranged from 4 to 8 MΩ. If series resistance in whole-cell mode exceeded 30MΩ, the cell was discarded from further analysis. For voltage-clamp experiments, cells were held at $^{-}$64mV after accounting for a liquid junction potential of −6.6mV. In current clamp recordings, resting potentials were relatively depolarized under our recording conditions and it was often necessary to inject hyperpolarizing current up to 20 pA to record stable light responses.

Light stimulation

All light stimuli were delivered episcopically through the 40x water immersion objective. Diffuse, full-field stimuli were generated by a xenon arc lamp with narrowband spectral filters and neutral density filters as previously described (Stabio, et al., 2018). The photon flux of unattenuated xenon light at 360, 480, and 520 nm were $1.7 \cdot 10^{16}$, $2.9 \cdot 10^{17}$, and $3.9 \cdot 10^{17}$ photons $\cdot$ cm^{-2} $\cdot$ s^{-1}, respectively as previously described (Stabio et al., 2018). In

some experiments, an iris was introduced into the xenon light path to create to smaller spots (either 165 μm or 620 μm diameter at the retinal surface). Spatially structured light stimuli for measuring area-response, spatial frequency and direction selectivity were generated using custom software written in Psychophysics Toolbox for Matlab driving an LCD projector (Optoma EP719) as described previously (Estevez et al., 2012). Finally, unless otherwise noted, intrinsic melanopsin-derived photoresponses were elicited via a 10 s step of full-field 100-W tungsten-halogen lamp passed through 480 nm narrow band spectral filter ($2.5 \cdot 10^{16}$ photons$\cdot s^{-1} cm^{-2}$)

Antibodies

Antibodies used are listed in Table 1. In all experiments involving melanopsin immunofluorescence, melanopsin immunodetection was amplified using tyramide signal amplification coupled with horseradish peroxidase (HRP)-paired with goat anti-rabbit IgG and an Alexa fluorophore. TSA-amplified anti-melanopsin and anti- choline acetyl transferase (ChAT) immunohistochemistry was performed as described previously (Estevez et al., 2012). For cells filled with lucifer yellow (LY), anti-LY immunohistochemistry was used to amplify the dye signal and the tissue was processed in combination with anti-ChAT as described in Estevez et al., 2012, to demarcate stratification. For stratification without interference from starburst amacrine somata, an anti-vesicular acetyl choline transferase (VaCHT) protocol was used as described previously (Huberman et al., 2009). Anti-GFP antibody was used to amplify the GFP signal in Chd3-GFP brain slices as described below.

Immunohistochemistry

Retinas were fixed for 30-45 minutes at room temperature in 4% paraformaldehyde (PFA) in 0.1 M phosphate buffer (PBS), washed thoroughly in PBS (6 × 10 min) at room temperature and incubated in blocking solution (2% Triton X-100 and 5% donkey serum in PBS) overnight at 4°C. Primary antibodies were incubated overnight at 4°C at concentrations indicated in Table 1with the exception of protocols including anti-melanopsin antibody, in which case the incubation period was 2 nights. Then, retinas were washed in PBS (6 × 10 min) and incubated in secondary antibody for 2-5 hours at concentrations indicated in Table 1. Retina's were washed in PBS (3 × 15 min), mounted on glass slides and imaged.

For immunofluorescence studies in brain, mice were sacrificed via transcardial perfusion with 4% PFA (Electron Microscopy Sciences). Brains were post-fixed in 4% PFA overnight. Brains were then rinsed with 0.1 M PBS, embedded in agarose, and 50 **μ**m coronal sections were made on a vibratome (Leica VT1000S). Brains from $Opn4^{cre/+}$;$Z/EG^{+/-}$ mice that were injected with retrograde tracers (as in Figure 8) were not further processed. Brains from Cdh3-GFP mice (as in Figure 1) were immunostained with anti- GFP antibody to amplify the GFP signal as follows: Floating sections were rinsed 3 × 10 min. in PBS and then incubated in blocking solution containing 10% normal goat serum (Vector Labs) and 0.5% Triton X-100 (Sigma-Aldrich) in PBS for 1 hour at room temperature. They were then incubated with rabbit-anti- GFP polyclonal antibody (Invitrogen) diluted 1:500 in blocking solution overnight at 4°C. Sections were rinsed 4 × 10 min in PBS, incubated in blocking solution for 45 minutes at room temperature, and then incubated in goat-anti-rabbit polyclonal secondary antibody (Alexa 488 conjugate, Invitrogen) for 3 hours at room

temperature. Sections were rinsed a final 4 × 10 min. in PBS and then mounted on slides and coverslipped with Aqua-mount (ThermoFisher Scientific). Visual brain areas were imaged on a fluorescence microscope (Nikon E600) with a digital camera (SPOT Imaging).

With regard to antibody specificity, the antibody against melanopsin was raised against a synthetic peptide consisting of the 15 N-terminal amino acids of mouse melanopsin. It produces no staining in melanopsin knockout mice (Opn4$^{-/-}$). Other antibodies were used to enhance fluorescence of exogenous fluorophores (GFP; Alexa Fluors). These clearly marked the same cells as before immunofluorescence labeling, indicating adequate specificity for our purposes. Likewise, antibodies for marking cholinergic processes (anti-VAChT; anti-ChAT) produced the highly characteristic parallel plexuses of processes near the middle of the IPL, as expected for selective staining of cholinergic (starburst) amacrine cells.

Image Analysis

Fluorescence images were acquired with an upright epifluorescence microscope (Nikon E600) equipped with a SPOT RT Slider digital camera (Diagnostic Instruments). Images of dye-filled neurons, obtained at multiple optical planes were imported into Adobe Photoshop layers and assembled into montages of the full dendritic field. From these we traced the somadendritic profile of each neuron in an overlay. Assessments of soma size were based on images acquired using minimal excitation intensity to avoid bloom. Analysis of soma diameter, dendritic field size, total dendritic length and counts of branch points were conducted in ImageJ (http://imagej.nih.gov) as previously described (Berson, Castrucci, & Provencio, 2010; Dhande et al., 2013; Estevez et al., 2012).

Confocal z-stacks were obtained from wholemount retinas and brain sections with a Zeiss LSM 510 Meta laser scanning microscope. Stacks were viewed and analyzed in ImageJ and Zeiss ZEN software. To generate side-view projections of retinal structures, we first digitally corrected image stacks for tissue warp with the Retina Flattener plugin of ImageJ (Stabio et al., 2018); https://github.com/mschiel/retinal-flattener/wiki see also (Sümbül et al., 2014). We typically used the ON and OFF starburst plexuses (ChAT bands) as the laminar references for the flattening process, but in some cases we relied on melanopsin immunopositive dendrites of M1 ipRGCs in the most distal IPL. High contrast images of the full dendritic profile of single cells viewed *en face* (in Figs. 2A and E; 5A and 7) were assembled from multiple partially overlapping maximum-intensity projections of the filled neuron which were then masked to hide features other than the cell of interest (e.g., background autofluorescence or processes of neighboring filled cells).

Data Analysis

Physiology data were analyzed as described previously (Dhande et al., 2013; Estevez et al., 2012) using Clampfit 9.2 (Molecular Devices), Origin 6.0 (Microcal Software) and Excel 2010 (Microsoft). Unless otherwise stated, error bars indicate SEM.

Results

Our goal was to provide a more complete accounting of the structure and function of retinal ganglion cells labeled in the Cdh3-GFP mouse, with particular emphasis on possible

intrinsic photosensitivity. In earlier reports (Osterhout et al., 2014; Osterhout et al., 2011), the Cdh3-GFP BAC transgene was expressed on an albino Swiss-Webster background. To develop a strain more favorable for analysis of light responses, we crossed these albino mice with C57BL6/J mice to obtain pigmented offspring carrying the Cdh3-GFP transgene on a mixed genetic background.

The pattern of GFP labeling in retinal neurons and retinofugal axons in adult pigmented mice was similar to that in albinos carrying this transgene (Osterhout et al., 2014; Osterhout et al., 2011). GFP fluorescence marked a moderate number of presumed ganglion cells in young pigmented mice, but this fraction declined with age, leaving at most only a few dozen RGCs with detectable GFP fluorescence in adult pigmented retinas; these were typically more prevalent in the ventral retina (Figure 1). Essentially the same set of retinofugal targets exhibited GFP-labeled terminals in pigmented as in albino mice: the olivary and posterior pretectal nuclei, and the intergeniculate leaflet and ventral divisions of the lateral geniculate nucleus (vLGN) (Figure 1). We confirmed the retinal origin of these labeled axons by demonstrating their absence two and a half weeks after eye removal (n = 3 animals; data not shown). Modest numbers of medium-field amacrine cells with somata in the inner nuclear layer were also labeled. These were usually much more brightly labeled than the RGCs and appeared likely to belong to a single type, but were not further characterized.

To study the morphology of GFP-positive ganglion cells, we targeted them for intracellular dye-filling, either by sharp micropipettes or during patch recording (n = 69 cells total). Analysis of dendritic branching and stratification patterns in these cells confirmed that they comprise two main types, as previously reported (Osterhout et al., 2014). Representative examples are shown in Figure 2. All intracellularly filled GFP+ cells in the ganglion-cell layer corresponded to one of these two morphological types. Both had relatively small cell bodies and highly branched processes, forming dendritic fields that were of intermediate size among mouse RGCs. The majority (86%) of these types (n = 59 of 69 filled cells) were bistratified, deploying dendrites near the inner and outer margins of the IPL (Figure 2a-c), in both the ON and OFF sublayers and at times diving between the two sublayers. The other, less abundant type (14%; n = 10 of 69 filled cells) was monostratified, with dendrites restricted to the inner ON sublayer (Figure 2e-f). The monostratified type appeared to correspond to the M5 subtype of ipRGCs (Stabio et al., 2018), as documented below.

The bistratified Cdh3-GFP cell is a novel melanopsin-expressing ipRGC type - the M6 cell

Patch-clamp recordings of the bistratified type revealed large, brisk inward currents and depolarization during either 5 s or 1 s full-field light flashes (Figure 6b and a, respectively). These ON responses were dramatically suppressed during pharmacological blockade of glutamatergic and fast ionotropic inhibitory neurotransmission, but a slow depolarizing ON response remained (Figure 6a, right). Such residual responses had the slow onset (time to peak = 6.3 +/− 0.8 ms, n = 9 M6 cells) and slow decay typical of the melanopsin-mediated responses of other ipRGCs. They were of modest maximal amplitudes (18.5 ± 5.5 pA; n = 9), comparable to those M4 and M5 cells, which express relatively low levels of melanopsin (Estevez et al., 2012; Stabio et al., 2018). Indeed, with tyramide signal amplification, weak melanopsin immunofluorescence was detectable in about half (46%; 13/28 cells tested) of

the bistratified GFP-positive cells, typically in the form of patchy labeling of the somatic surface (Figure 2d). Their dendrites were never labeled and if amplification was omitted, even their somata lacked detectable melanopsin immunofluorescence, even when an intrinsic response was demonstrated electrophysiologically during patch clamp recordings.

Thus, the predominant GFP-positive cell in Cdh3-GFP mice appears to constitute a novel ipRGC type, readily distinguishable from the established ipRGC types, M1-M5. We will therefore refer to them as 'M6 cells.' We reasoned that if these bistratified Cdh3-GFP cells were expressing melanopsin, they should be represented among the GFP+ cells in a melanopsin reporter mouse ($Opn4^{cre/+}$; $Z/EG^{+/-}$; Ecker et al., 2010). They were, as documented by dye filling in the $Opn4^{cre/+}$; $Z/EG^{+/-}$ mouse line for a dozen representative cells shown in Figure 3b.

Morphology of M6 cells

A total of 34 of the 69 filled bistratified cells from the Cdh3-GFP mouse line were manually traced and analyzed for morphological parameters. The dendritic fields of these M6 cells were smaller on average than those of previously identified ipRGC types (216 ± 30 μm equivalent diameter; mean ± s.d., n = 34; Figure 4), and their cell bodies were also among the smallest of the ipRGCs (12.7 μm ± 1.8 μm, n = 34; mean ± s.d). M6 cells had highly branched, relatively compact arbors of fine spiny dendrites (Figure 3); thus, they had many more total dendritic branchpoints than other ipRGC types (100 ± 27, n=34; mean ± s.d.; Figure 4d-e). Total dendritic length was 3618 ± 892 (n=34; mean ± s.d.). The dendritic branches assumed a wide range of orientations relative to the cell body, often crossing over other branches or curving back toward the soma, giving the cells a tangled, bushy appearance.

The inner dendritic arbor of M6 cells was generally much more extensive than the outer arbor, accounting for 84 ± 12% of the cell's total dendritic length (mean ± s.d.; n = 34). The inner arbor was relatively broadly distributed in depth, spanning roughly the inner two thirds of the ON sublamina of the IPL. Processes in this arbor extended from just below the ON cholinergic band to the ganglion-cell layer (Fig 2b,c and 5c). Dendrites within the inner arbor frequently crossed over one another when viewed in profile (Figure 3), but were nearly always well separated in depth within the ON sublayer. Dendritic spines and short, fine dendritic branches were a prominent feature of the inner arbor of most optimally dye-filled M6 cells (Figure 5b,d and f); though not apparent in every M6 cell, they were certainly more commonly encountered in these cells than in M1 – M5 ipRGCs.

The outer arbor of M6 cells was generally much less extensive (16 ± 12% of total dendritic length; mean ± s.d.; n = 34) and often more compact than the ON arbor, confined to one or more small subregions within the dendritic field. The outer dendrites stratified narrowly near the distal margin of the IPL, well distal to the OFF cholinergic band and very close to the cell bodies of the inner nuclear layer (Figures 2c and 5c). There, they co-stratified with the dendrites of M1 ipRGCs, as we confirmed by melanopsin immunostaining, which clearly reveals M1 dendrites (Figure 2b, 5c). In some M6 cells, a fraction of the ON arbor was recurrent or 'diving', having first ascended to outer arbor before descending once more

through the IPL to rejoin the inner arbor (blue processes in Figure 2a and 3). Though a common feature of M6 cells, it was not universal.

Physiological properties of M6 cells

In control bath solution, with chemical synapses functionally intact, M6 cells exhibited sustained ON responses to full-field illumination (Figure 6 a, b, c). Synaptically-driven light responses were entirely eliminated by bath application of L-AP4, which blocks the ON channel (n = 4, data not shown). In the presence of a synaptic block cocktail including LAP-4, AP-5 and DNQX), a slow, weak intrinsic light response evidently mediated by melanopsin phototransduction could be observed in response to long (10 s or 20 s) steps of 480 nm light in both voltage clamp and current clamp recordings (Figure 6a, right).

M6 cells had strong suppressive surrounds in their receptive fields because large spots were much less effective than spots of intermediate size. The highest frequency of spikes occurred in response to spot sizes between 200 – 400 μm. However, the optimal spot diameter was approximately 390 μm (Figure 6b) which is nearly twice the mean dendritic field diameter (~200 μm). Surround suppression was also reflected in substantial attenuation of the response to whole-field drifting gratings at low spatial frequencies (Figure 6c). A total of 27 M6 cells were tested for chromatic opponency; nearly all of these cells lacked opponency. Narrowband spectral stimuli of 360 or 520 nm, which differentially activate the two cone opsins, evoked the same polarity of response, even for full field stimuli (Figure 6d). There were three outliers among these cells which showed a weak outward response in response to a large 520 nm flash of light. M6 cells also lacked obvious direction selectivity (Figure 6e), though they sometimes showed weak axial motion tuning, preferring a particular axis of grating motion but not one direction of motion along that axis over the other).

M5 cells are labeled in the Cdh3-GFP mouse

The monostratified variety of GFP-positive cell in the Cdh3 mouse (Figure 2e,f) appears to correspond to the M5 type of ipRGC (Stabio et al., 2018). Four additional examples of such cells appear in Figure 7a and e. These closely matched M5 cells both anatomically and physiologically. Their dendritic were invariably restricted to the inner ON sublayer of the IPL, proximal to (below) the ON cholinergic plexus (Figure 2f and Figure 7b), as expected for M5 cells. Their dendritic field sizes were of appropriate size (283 ± 21 μm; n = 8). A distinctive functional property of M5 cells is their chromatic opponency when tested with full-field narrowband spectral stimuli (Stabio et al., 2018), and we confirmed this for one of the monostratified Cdh3-GFP cells (Figure 7a,c). Though we recorded four other presumptive M5 cell marked by GFP in Cdh3-GFP-positive cell that lacked obvious chromatic opponency, this is not surprising; M-cone opsin expression is very weak in the ventral retina, where most Cdh3-GFP cells are found in adult mice. In addition, as expected (Stabio et al., 2018), monostratified Cdh3-GFP cells exhibited intrinsic light responses under synaptic blockade (n = 5; Figure 7d). Among mouse ganglion cells, only M5 cells are known to possess all of these attributes. M5 cells are relatively rare among the GFP-tagged neurons in the Cdh3 mouse; among 69 filled GFP+ ganglion cells in our sample, only 10 (14%) were presumptive M5 cells, while 59 (86%) were M6 cells.

M6 cells innervate the dorsal lateral geniculate nucleus

GFP-positive retinal axons were detectable in the dLGN in pigmented Cdh3-GFP mice, especially in the early postnatal period (Figure 1, right column). Although these were greatly reduced in number in adult animals, they clearly persisted until at least P30 (Figure 1, bottom right), and were located at that age in a restricted zone roughly midway between the overlying optic tract and the internal margin of the nucleus. We recently demonstrated that M5 ipRGCs project to the dLGN (Stabio et al., 2018). Because M5 cells comprise a minority of fluorescent ganglion cells in Cdh3-GFP mice, these retinogeniculate afferents could derive from M5 rather than from M6 cells. To provide convergent evidence on whether M6 cells might also innervate the dLGN, we made deposits of a retrograde tracer, cholera toxin β-subunit conjugated to Alexa Fluor 594 (Figure 8a), restricted to the dLGN of melanopsin GFP reporter mice ($Opn4^{cre/+}$;$Z/EG^{+/-}$). Retrolabeled cells that were also GFP+ (and thus presumptive ipRGCs) were targeted for intracellular dye filling (Figure 8b). Cells with characteristic M6 morphology were clearly among the retrolabeled, dye-filled cells (Figure 8c).

We confirmed this finding by a second approach as performed previously for M5 cells (Stabio et al., 2018). Specifically, we performed intraocular injections of a Cre-dependent AAV2 virus in the eyes of Opn4cre/+;Z/EG+/− mice; this induced GFP expression in infected Cre-expressing cells (which in this mouse line were ipRGCs). Then, we injected the dLGN of these mice unilaterally with red fluorescent latex microspheres (“beads”), a retrograde tracer that, unlike CTB, is thought to be taken up mainly at terminals rather and not by passing fibers. We looked for cells in the retina that were co-labeled with GFP and beads and reconstructed dozens of them fully enough to establish their ipRGC subtype identity based on morphological properties (Fig. 4). Several of these were clearly M6 cells. Fig. 8G shows a particular completely reconstructed example.

Discussion

We introduce a novel type of intrinsically photosensitive retinal ganglion cell of the mouse retina, the M6 cell. Though M6 cells differ in several respects from all previously described ipRGC types in mouse, clearly belong within the ipRGC class. They apparently express at least some melanopsin, as reflected by their weak intrinsic photosensitivity, their labeling in a melanopsin reporter mouse, and the modest melanopsin immunostaining sometimes detectable in their somatic membrane.

One structural feature that distinguishes this type from nearly all previously described ipRGC types is its highly-branched, bistratified dendritic arbor. Nearly all other ipRGC types are monostratified (Fig. 9). Most stratify exclusively in the inner ON sublayer of the IPL (M2, M4 and M5 cells), while M1 ipRGCs stratify only in the outermost OFF sublayer (M1). The only previously described ipRGC that shares the property of bistratification with M6 cells is the M3 type. M3 cells deploy their dendrites in the same two strata as M6 cells (and ipRGCs overall). However, the two types are easily distinguishable because M6 cells have much smaller and more highly branched dendritic arbors which are typically spiny. In addition, M3 cells express more melanopsin than M6 cells, as reflected in stronger

somadendritic melanopsin immunoreactivity and larger melanopsin-dependent intrinsic light responses (Schmidt & Kofuji, 2011; Zhao, Stafford, Godin, King, & Wong, 2014).

As a practical matter, M6 cells are more likely to be mistaken for M5 cells than for M3 cells. The outer dendritic arbor of M6 cells can be overlooked; it is delicate, generally much less extensive than the inner arbor, and in extreme cases consists of just a handful of short dendrites. The more prominent inner arbor of the M6 cell is only subtly different from that of M5 cells. Both are highly branched and compact and they stratify at the same IPL depth – in the inner part of the ON sublayer, proximal to the ON ChAT band. M5 and M6 cells also both have relatively small cell bodies. However, M5 cells can be distinguished from M6 cells by several criteria. These include their lack of any dendrites in the OFF sublamina, their slightly less highly branched and spiny dendritic profiles, and their spectrally opponent responses to narrowband stimuli (UV-ON; green-OFF;(Stabio et al., 2018)). Technical factors may have limited our ability to detect spectral tuning in M6 cells. Due to our heavy reliance on the Cdh3-GFP mouse, our sample of M6 cells was drawn mainly from the ventral retina, where M-opsin expression is weak. Furthermore, M opsin may have been differentially bleached by the blue epifluorescence beam used to locate GFP+ cells. On the other hand, we were able to detect chromatic opponency in M5 cells in both Cdh3-GFP mice and in melanopsin-reporter mice under the same recording conditions, and failed to detect it in M6 cells (n = 4, data not shown) recorded in the melanopsin reporter mouse. Still, the question should be revisited in the dorsal retina, ideally using multiphoton imaging to minimize the effects of pigment bleaching.

Significance of dendritic stratification of M6 cells

Like all ipRGC types, the M6 cell appears to be an ON sustained cell. This pure-ON response signature is atypical of bistratified ganglion cells, which generally are ON-OFF cells, as typified by the ON-OFF direction-selective cells. We never observed OFF responses, whether we dimmed the light in across the whole field or only within the receptive-field center, and whether we used UV or green narrowband stimuli. Blockade of the ON channel completely abolished light-evoked responses other than the intrinsic, melanopsin-based photoresponse. However, M3 cells offer a clear precedent for pure ON responses in a bistratified ganglion cell. It is noteworthy that the dendrites of these two types perfectly costratify. Similarly, M1 cells are also pure-ON cells, despite stratifying exclusively at the outer (distal) margin of the IPL, at the same level as the outer arbors of M3 and M6 cells. This raises the possibility that bipolar inputs to the outer arbor of M6 cells might be the target of the same unusual ON channel input as M1 ipRGCs and dopaminergic amacrine cells (Dumitrescu, Pucci, Wong, & Berson, 2009; Hoshi, Liu, Massey, & Mills, 2009; Kim et al., 2012). These consist of ribbon synaptic outputs from ON cone bipolar axons, either *en passant* or on short side branches, forming what can be considered an accessory ON sublamina of the IPL. The inner dendritic arbor of M6 cells almost certainly receives strong excitatory drive from ON bipolar cells too. Judging from their level of stratification, M6 dendrites seem in a position to receive contacts from ON cone bipolar cell types 6, 7, 8 and 9.

Among the targets of ectopic ON bipolar *en passant* synapses in rabbit retina are outer (distal) dendrites of the "bistratified diving cell" (Hoshi et al., 2009). This type is strikingly similar to the M6 cell. Both have bistratified arbors concentrated at the two margins of the IPL. Both have a dominant inner arbor, a more modest outer one, and recursive ('diving') dendrites that return to the inner arbor after contributing to the outer one. Both have prominent dendritic spines and pure ON light responses. In mouse retina, numerous bistratified RGC types have been documented either in anatomical studies (Badea & Nathans, 2004; Coombs, van der List, Wang, & Chalupa, 2006; Ivanova, Lee, & Pan, 2013; Schubert, Maxeiner, Kruger, Willecke, & Weiler, 2005; Volgyi, Chheda, & Bloomfield, 2009) or in structure-function studies (Lee, Zhang, Chen, & Zhou, 2016; Sabbah, Berg, Papendorp, Briggman, & Berson, 2017; Tien, Kim, & Kerschensteiner, 2016). Most seem not to precisely match the M6 cell in at least one feature, such as stratification or dendritic field size. One exception is the middle bistratified (m-BSC) type of RGC in the PCP2-Cre mouse. This shares with M6 cells an ON dominated bistratified arbor, ramifying outside the ChAT bands, and intermediate-size dendritic field, and a small soma. The PCP2-Cre line could thus be a valuable tool for further studies of M6 cells, including their functional roles in vision. The M13 cell of Coombs et al. (2006) matches M6 cells in most respects, but apparently lacks the ON dominance of the dendritic arbor that is typical of M6 cells.

Cdh3-GFP reporter mouse reveals central projections of M6 and M5 ipRGCs

Every dye-filled GFP+ ganglion cell in our pigmented strain of Cdh3-GFP mice fell neatly into one of two morphological types. The great majority (86%) were M6 cells and the remainder were M5 cells. This parallels the distinction drawn by Osterhout et al. (2014) between Type 1 monostratified and Type 2 bistratified GFP+ cells in their Cdh3-GFP strain. Thus, GFP-positive optic axons in our strain derive mostly from M6 cells, with a small minority from M5 cells. Collectively, the central distribution of these axons resembles that previously described for albino Cdh3-GFP mice, targeting mainly the olivary and posterior pretectal nuclei and several distinct regions within each component of the LGN (vLGN, intergeniculate leaflet, and dLGN) (Osterhout et al., 2014; Osterhout et al., 2011). Our data thus indicate that these brain regions receives input from at least one of these ipRGC types and possibly both (Fig. 9). With respect to the dLGN, the GFP-positive retinogeniculate terminal field there is in accord with our earlier evidence that M5 cells innervate the dLGN (Stabio et al., 2018). And we have shown here that M6 cells, too, can be retrolabeled from the dLGN. Thus, it appears likely that the GFP+ terminal field in the dLGN of Cdh3-GFP mice represents a mixed M5/M6 input.

A striking feature of this terminal field is its restricted distribution within the dLGN. This partly a consequence of retinotopy; the dLGN labeling appears in the expected region of the geniculate map (Piscopo, El-Danaf, Huberman, & Niell, 2013), given the preferential concentration of GFP-labeled RGCs in the ventral retina. However, the restriction of the geniculate terminal field in laminar depth (distance from the overlying optic tract) appears be related to the segregation of specific types of retinogeniculate axons, derived from distinct RGC types, in different latent laminae of the dLGN. The Cdh3-GFP terminal field lies roughly midway between the external and internal margins of the nucleus, well internal to the lamina preferentially targeted by ON-OFF direction selective ganglion cells

(Huberman et al., 2009; Rivlin-Etzion et al., 2011) but also well external to the layer of dense input from ipRGC overall (Ecker et al., 2010). This geniculate lamina is thus a target not only of sustained ON signals derived in part from melanopsin (M5 and possible M6), but also of cone-opponent chromatic signals (M5 cells; (Stabio et al., 2018)). A reporter for all ipRGC types (M1-M6; (Ecker et al., 2010)) mostly strongly labels the internal half of the dLGN, and the Cdh3-GFP terminals would appear to account for only those afferents among this blend terminating closer to the optic tract. Likewise, M1 ipRGCs can be largely excluded as a source of the remaining deep (internal) ipRGC terminal layer. This implies that M4 cells (ON-alpha cells) are the major source of this input (Estevez et al., 2012), which seems to match the laminar position of afferents from the transient OFF alpha cell (Huberman et al., 2008).

These data also shed new light on the nature of retinal input to the olivary pretectal nucleus. This is well known as a target of ipRGCs, but the focus to date has been on the pupillary pathway, and the contribution of the original M1 type of ipRGC to the pupillary light reflex. However, this input appears to target the shell of the OPN, whereas its core receives input from other RGCs (Hattar et al., 2006). The identity of retinal afferents to the OPN core is largely unknown, though it certainly includes some ipRGCs (Ecker et al., 2010). Our findings indicate that the core must receive input from M5 or M6 ipRGCs, and possibly both.

Though these data underscore the value of the Cdh3-GFP mouse, some caution is warranted in exploiting this model. Though it is an efficient way to target M6 cells for study, it labels these cells only in the ventral retina. If, as expected, M6 cells tile the retina, many remain unlabeled in this reporter mouse. Nor is this reporter selective for M6 cells, since some GFP + cells are M5 ipRGCs. These are so rare that the Cdh3-GFP mouse is not particularly helpful for targeting M5 cells. The numbers of RGCs labeled by the Cdh3 transgene and possibly the cell types represented appear somewhat labile over development and/or different genetic backgrounds (Osterhout et al., 2014; Osterhout et al., 2011; Sümbül et al., 2014)). The number of GFP positive cells drops dramatically in early postnatal development (Figure 1) and certain targets innervated by the GFP+ cells shortly after birth (superior colliculus and MTN) lack such innervation in mature mice. M2 ipRGCs can apparently be labeled in some Cdh3-GFP strains. Osterhout et al. (2014) found that about 10% GFP-tagged RGCs in their albino strain of Cdh3-GFP mice were robustly melanopsin immunopositive. These are presumably at least partly M2 ipRGCs, judging from the substantial melanopsin immunolabeling of their dendrites (which is never seen in M5 or M6 cells) and from the stratification of those dendrites exclusively in the inner ON sublamina, both expected for M2 cells (see Osterhout et al., 2011, their Figure 3). Similarly, Sümbül et al., (2014) characterized GFP-positive RGCs in Cdh3 mice as monostratified ON cells; that pattern of stratification could match those of either M2 cells (which we never found to be GFP+ in adult mice of the strain we used) or M5 cells (which comprises only a small minority of the GFP+ cells in our strain). Some smaller, bushy dendritic profiles illustrated in their Supplementary Figure 17 appear consistent with M5 cells, other sparser ones with M2 cells.

Acknowledgements:

Special thanks to Dianne Boghossian and Kimberly Boghossian for assistance maintaining and genotyping mice. Funding was provided by NIH Grants F32-EY021994 (M.E.S.), R01-EY012793 (D.M.B.) and NSF Grant I2011104359 (P.M.F.).

References

Badea TC, & Nathans J (2004). Quantitative analysis of neuronal morphologies in the mouse retina visualized by using a genetically directed reporter. J Comp Neurol, 480(4), 331–351. doi:10.1002/cne.20304 [PubMed: 15558785]

Baver SB, Pickard GE, Sollars PJ, & Pickard GE (2008). Two types of melanopsin retinal ganglion cell differentially innervate the hypothalamic suprachiasmatic nucleus and the olivary pretectal nucleus. Eur J Neurosci, 27(7), 1763–1770. doi:10.1111/j.1460-9568.2008.06149.x [PubMed: 18371076]

Berson DM, Castrucci AM, & Provencio I (2010). Morphology and mosaics of melanopsin-expressing retinal ganglion cell types in mice. J Comp Neurol, 518(13), 2405–2422. doi:10.1002/cne.22381 [PubMed: 20503419]

Brown TM, Gias C, Hatori M, Keding SR, Semo M, Coffey PJ, … Lucas RJ (2010). Melanopsin contributions to irradiance coding in the thalamo-cortical visual system. PLoS Biol, 8(12), e1000558. doi:10.1371/journal.pbio.1000558 [PubMed: 21151887]

Coombs J, van der List D, Wang GY, & Chalupa LM (2006). Morphological properties of mouse retinal ganglion cells. Neuroscience, 140(1), 123–136. doi:10.1016/j.neuroscience.2006.02.079 [PubMed: 16626866]

Dhande OS, Estevez ME, Quattrochi LE, E1-Danaf RN, Nguyen PL, Berson DM, & Huberman AD (2013). Genetic dissection of retinal inputs to brainstem nuclei controlling image stabilization. J Neurosci, 33(45), 17797–17813. doi:10.1523/JNEUROSCI.2778-13.2013 [PubMed: 24198370]

Dumitrescu ON, Pucci FG, Wong KY, & Berson DM (2009). Ectopic retinal ON bipolar cell synapses in the OFF inner plexiform layer: contacts with dopaminergic amacrine cells and melanopsin ganglion cells. J Comp Neurol, 517(2), 226–244. doi:10.1002/cne.22158 [PubMed: 19731338]

Ecker JL, Dumitrescu ON, Wong KY, Alam NM, Chen SK, LeGates T, … Hattar S (2010). Melanopsin-expressing retinal ganglion-cell photoreceptors: cellular diversity and role in pattern vision. Neuron, 67(1), 49–60. doi:S0896-6273(10)00419-8 [pii] 10.1016/j.neuron.2010.05.023 [PubMed: 20624591]

Estevez ME, Fogerson PM, Ilardi MC, Borghuis BG, Chan E, Weng S, … Berson DM (2012). Form and function of the M4 cell, an intrinsically photosensitive retinal ganglion cell type contributing to geniculocortical vision. J Neurosci, 32(39), 13608–13620. [PubMed: 23015450]

Hattar S, Kumar M, Park A, Tong P, Tung J, Yau KW, & Berson DM (2006). Central projections of melanopsin-expressing retinal ganglion cells in the mouse. J Comp Neurol, 497(3), 326–349. [PubMed: 16736474]

Hattar S, Liao HW, Takao M, Berson DM, & Yau KW (2002). Melanopsin-containing retinal ganglion cells: architecture, projections, and intrinsic photosensitivity. Science, 295(5557), 1065–1070. doi:10.1126/science.1069609 [PubMed: 11834834]

Hoshi H, Liu WL, Massey SC, & Mills SL (2009). ON inputs to the OFF layer: bipolar cells that break the stratification rules of the retina. J Neurosci, 29(28), 8875–8883. doi:10.1523/JNEUROSCI.0912-09.2009 [PubMed: 19605625]

Hu C, Hill DD, & Wong KY (2013). Intrinsic physiological properties of the five types of mouse ganglion-cell photoreceptors. J Neurophysiol, 109(7), 1876–1889. doi:10.1152/jn.00579.2012 [PubMed: 23343892]

Huberman AD, Manu M, Koch SM, Susman MW, Lutz AB, Ullian EM, … Barres BA (2008). Architecture and activity-mediated refinement of axonal projections from a mosaic of genetically identified retinal ganglion cells. Neuron, 59(3), 425–438. doi:10.1016/j.neuron.2008.07.018 [PubMed: 18701068]

Huberman AD, Wei W, Elstrott J, Stafford BK, Feller MB, & Barres BA (2009). Genetic identification of an On-Off direction-selective retinal ganglion cell subtype reveals a layer-specific subcortical

map of posterior motion. Neuron, 62(3), 327–334. doi:10.1016/j.neuron.2009.04.014 [PubMed: 19447089]

Ivanova E, Lee P, & Pan ZH (2013). Characterization of multiple bistratified retinal ganglion cells in a purkinje cell protein 2-Cre transgenic mouse line. J Comp Neurol, 521(9), 2165–2180. doi: 10.1002/cne.23279 [PubMed: 23224947]

Kim HL, Jeon JH, Koo TH, Lee UY, Jeong E, Chun MH, … Kim IB (2012). Axonal synapses utilize multiple synaptic ribbons in the mammalian retina. PLoS One, 7(12), e52295. doi:10.1371/journal.pone.0052295 [PubMed: 23284975]

Lee S, Zhang Y, Chen M, & Zhou ZJ (2016). Segregated Glycine-Glutamate Co-transmission from vGluT3 Amacrine Cells to Contrast-Suppressed and Contrast-Enhanced Retinal Circuits. Neuron, 90(1), 27–34. doi:10.1016/j.neuron.2016.02.023 [PubMed: 26996083]

Novak A, Guo C, Yang W, Nagy A, & Lobe CG (2000). Z/EG, a double reporter mouse line that expresses enhanced green fluorescent protein upon Cre-mediated excision. Genesis, 28(3-4), 147–155. [PubMed: 11105057]

Osterhout JA, El-Danaf RN, Nguyen PL, & Huberman AD (2014). Birthdate and outgrowth timing predict cellular mechanisms of axon target matching in the developing visual pathway. Cell Rep, 8(4), 1006–1017. doi:10.1016/j.celrep.2014.06.063 [PubMed: 25088424]

Osterhout JA, Josten N, Yamada J, Pan F, Wu SW, Nguyen PL, … Huberman AD (2011). Cadherin-6 mediates axon-target matching in a non-image-forming visual circuit. Neuron, 71(4), 632–639. doi:10.1016/j.neuron.2011.07.006 [PubMed: 21867880]

Piscopo DM, El-Danaf RN, Huberman AD, & Niell CM (2013). Diverse visual features encoded in mouse lateral geniculate nucleus. J Neurosci, 33(11), 4642–4656. doi:10.1523/JNEUROSCI.5187-12.2013 [PubMed: 23486939]

Pu M, Berson DM, & Pan T (1994). Structure and function of retinal ganglion cells innervating the cat's geniculate wing: an in vitro study. J Neurosci, 14(7), 4338–4358. [PubMed: 8027783]

Rivlin-Etzion M, Zhou K, Wei W, Elstrott J, Nguyen PL, Barres BA, … Feller MB (2011). Transgenic mice reveal unexpected diversity of on-off direction-selective retinal ganglion cell subtypes and brain structures involved in motion processing. J Neurosci, 31(24), 8760–8769. doi:10.1523/JNEUROSCI.0564-11.2011 [PubMed: 21677160]

Sabbah S, Berg D, Papendorp C, Briggman KL, & Berson DM (2017). A Cre Mouse Line for Probing Irradiance- and Direction-Encoding Retinal Networks. eNeuro, 4(2). doi:10.1523/ENEURO.0065-17.2017

Schmidt TM, Chen SK, & Hattar S (2011). Intrinsically photosensitive retinal ganglion cells: many subtypes, diverse functions. Trends Neurosci, 34(11), 572–580. doi:S0166-2236(11)00105-6 [pii] 10.1016/j.tins.2011.07.001 [PubMed: 21816493]

Schmidt TM, & Kofuji P (2011). Structure and function of bistratified intrinsically photosensitive retinal ganglion cells in the mouse. J Comp Neurol, 519(8), 1492–1504. doi:10.1002/cne.22579 [PubMed: 21452206]

Schubert T, Maxeiner S, Kruger O, Willecke K, & Weiler R (2005). Connexin45 mediates gap junctional coupling of bistratified ganglion cells in the mouse retina. J Comp Neurol, 490(1), 29–39. doi:10.1002/cne.20621 [PubMed: 16041717]

Sonoda T, & Schmidt TM (2016). Re-evaluating the Role of Intrinsically Photosensitive Retinal Ganglion Cells: New Roles in Image-Forming Functions. Integr Comp Biol, 56(5), 834–841. doi: 10.1093/icb/icw066 [PubMed: 27371393]

Stabio ME, Sabbah S, Quattrochi LE, Ilardi MC, Fogerson PM, Leyrer ML, … Berson DL (2018). The M5 Cell: A Color-Opponent Intrinsically Photosensitive Retinal Ganglion Cell. Neuron, 97(1), 251. doi:10.1016/j.neuron.2017.12.030 [PubMed: 29301102]

Sümbül U, Song S, McCulloch K, Becker M, Lin B, Sanes JR, … Seung HS (2014). A genetic and computational approach to structurally classify neuronal types. Nat Commun, 5, 3512. doi: 10.1038/ncomms4512 [PubMed: 24662602]

Tien NW, Kim T, & Kerschensteiner D (2016). Target-Specific Glycinergic Transmission from VGluT3-Expressing Amacrine Cells Shapes Suppressive Contrast Responses in the Retina. Cell Rep, 15(7), 1369–1375. doi:10.1016/j.celrep.2016.04.025 [PubMed: 27160915]

Van Hook MJ, Wong KY, & Berson DM (2012). Dopaminergic modulation of ganglion-cell photoreceptors in rat. Eur J Neurosci, 35(4), 507–518. doi:10.1111/j.1460-9568.2011.07975.x [PubMed: 22304466]

Volgyi B, Chheda S, & Bloomfield SA (2009). Tracer coupling patterns of the ganglion cell subtypes in the mouse retina. J Comp Neurol, 512(5), 664–687. doi:10.1002/cne.21912 [PubMed: 19051243]

Wong KY, Dunn FA, & Berson DM (2005). Photoreceptor adaptation in intrinsically photosensitive retinal ganglion cells. Neuron, 48(6), 1001–1010. doi:10.1016/j.neuron.2005.11.016 [PubMed: 16364903]

Wong KY, Dunn FA, Graham DM, & Berson DM (2007). Synaptic influences on rat ganglion-cell photoreceptors. J Physiol, 582(Pt 1), 279–296. doi:10.1113/jphysiol.2007.133751 [PubMed: 17510182]

Zhao X, Stafford BK, Godin AL, King WM, & Wong KY (2014). Photoresponse diversity among the five types of intrinsically photosensitive retinal ganglion cells. J Physiol, 592(Pt 7), 1619–1636. doi:10.1113/jphysiol.2013.262782 [PubMed: 24396062]

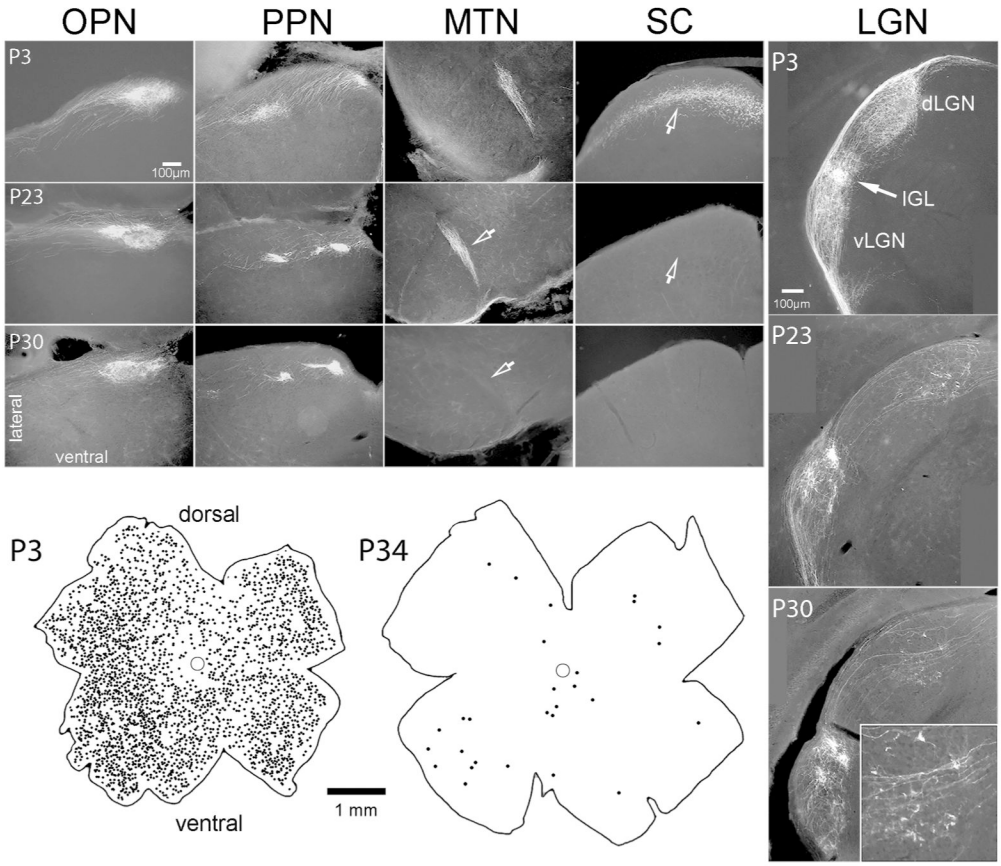

Figure 1.

Distribution of GFP+ ganglion cells and their axons in pigmented Cdh3-GFP mice from near birth to maturity. Photomicrographs show the termination of GFP+ axons within five separate retinorecipient nuclei of the brainstem and thalamus at three postnatal ages. Representative data are shown among P3 (n =2), P23 (n = 2) and P30 (n = 4). These are of retinal origin because they disappear after enucleation (n = 3 mice; data not shown). Note that sparse, localized retinogeniculate innervation persists in juvenile mice (P30; inset shows a high magnification view of these terminals). Drawings below show the distribution of GFP-positive retinal ganglion cells in these mice shortly after birth (left) and at maturity (right). Only GFP cells in the ganglion-cell layer are plotted; the brightly labeled amacrine cells have been excluded.

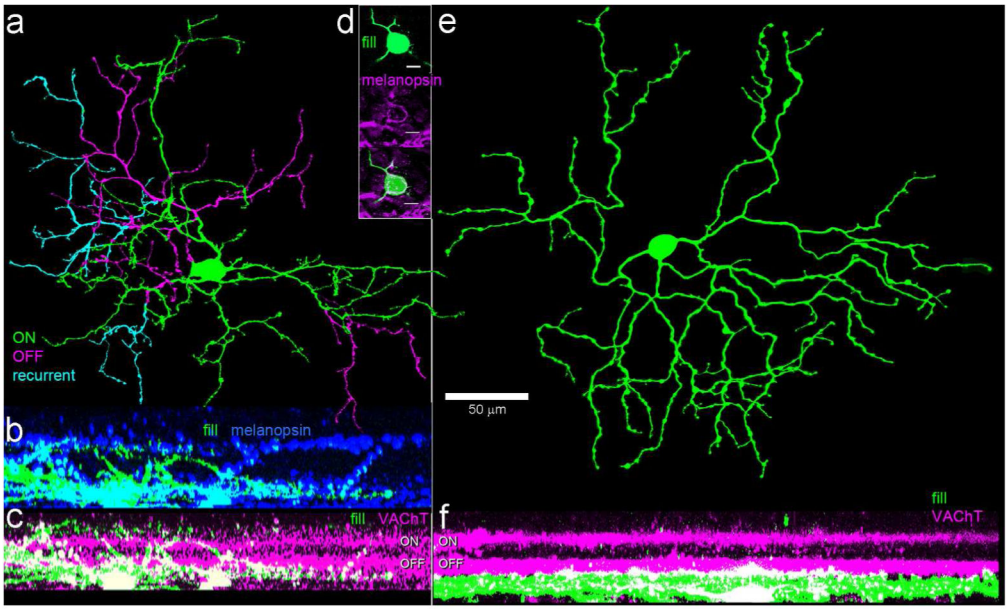

Figure 2.

Morphology, dendritic stratification and melanopsin immunoreactivity of the two ganglion-cell types encountered among GFP-positive RGCs in Cdh3-GFP mice. Cells were targeted for dye filling based on GFP fluorescence. (a-c) Morphology of the preponderant cell type, a bistratified cell with a relatively small arbor of spiny dendrites. a: a pseudocolored view of the bistratified type as viewed *en face* ; green and cyan dendrites are in the ON sublayer, magenta in the OFF sublayer. Cyan dendrites are recurrent, returning to the ON sublayer having traveled at least a small distance in the OFF sublayer. Scale bar (50 µm) applies to (a) and (e). (b-c) Side view projections of this filled cell in relation to the two strata of melanopsin-immunopositive dendrites (blue) or the cholinergic bands, revealed by anti-VAChT immunolabeling (magenta). (d) Example of the somatic anti-melanopsin immunoreactivity observed in a fraction of the somas of cells of this type. Scale bar: 10 µm. (e-f) Morphology of the monostratified GFP-positive RGC type in the Cdh3-GFP mouse, apparently equivalent to the M5 ipRGC type (Stabio et al., 2018). (e) An *en face* view color coded as in (a); all dendrites stratify in the ON sublayer (green). (f) Side view projection, showing stratification almost entirely below the ON cholinergic band.

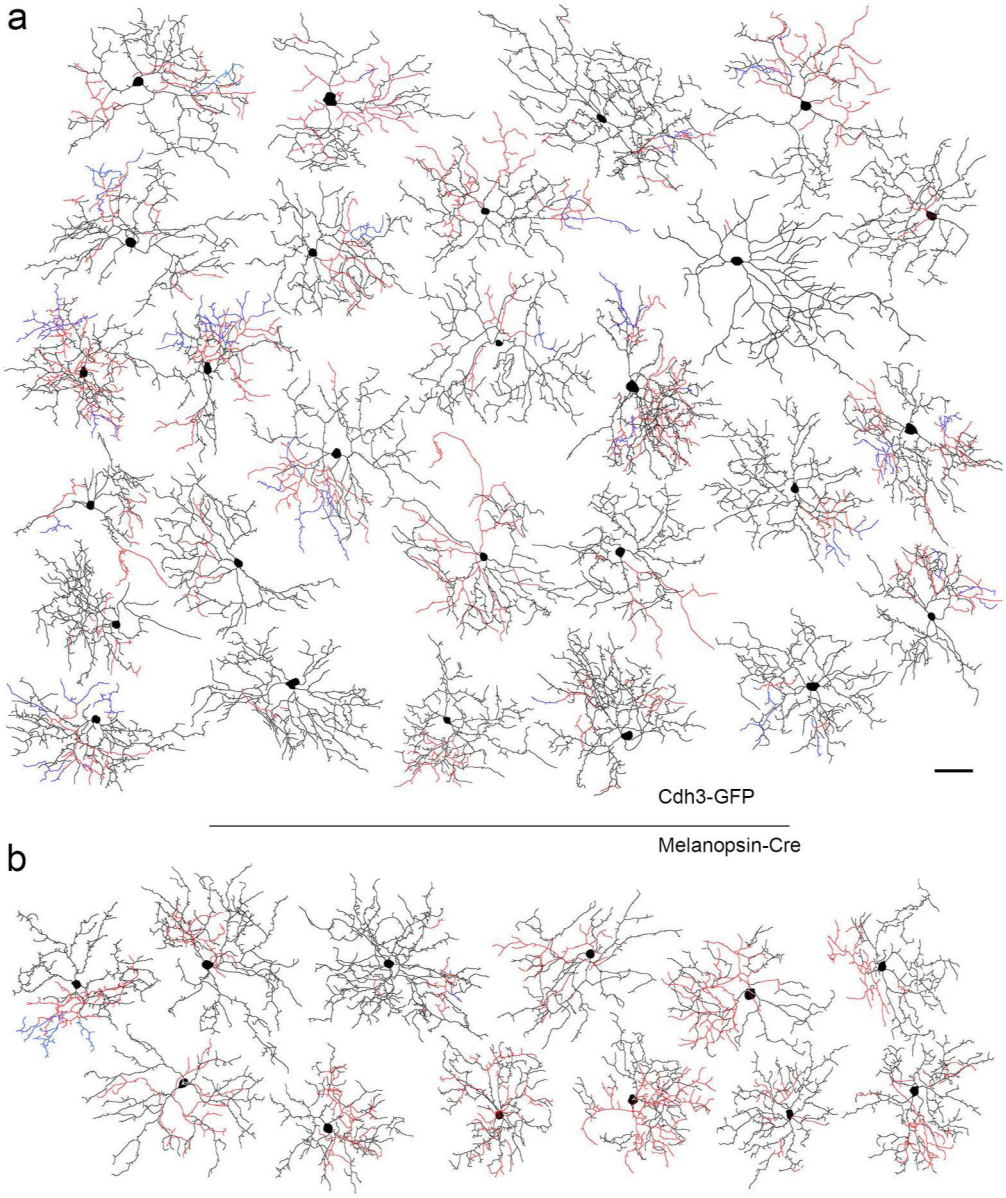

Figure 3.

Tracings of intracellularly dye-filled M6 ipRGCs targeted either in the Cdh3-GFP (a) or melanopsin reporter mice (b). Dendrites in the ON sublayer are indicated in dark hues (black/blue), while those in the OFF sublayer are in red. Blue processes are recurrent, returning to the ON sublayer after traveling through the OFF sublayer. Scale bar: 50 μm

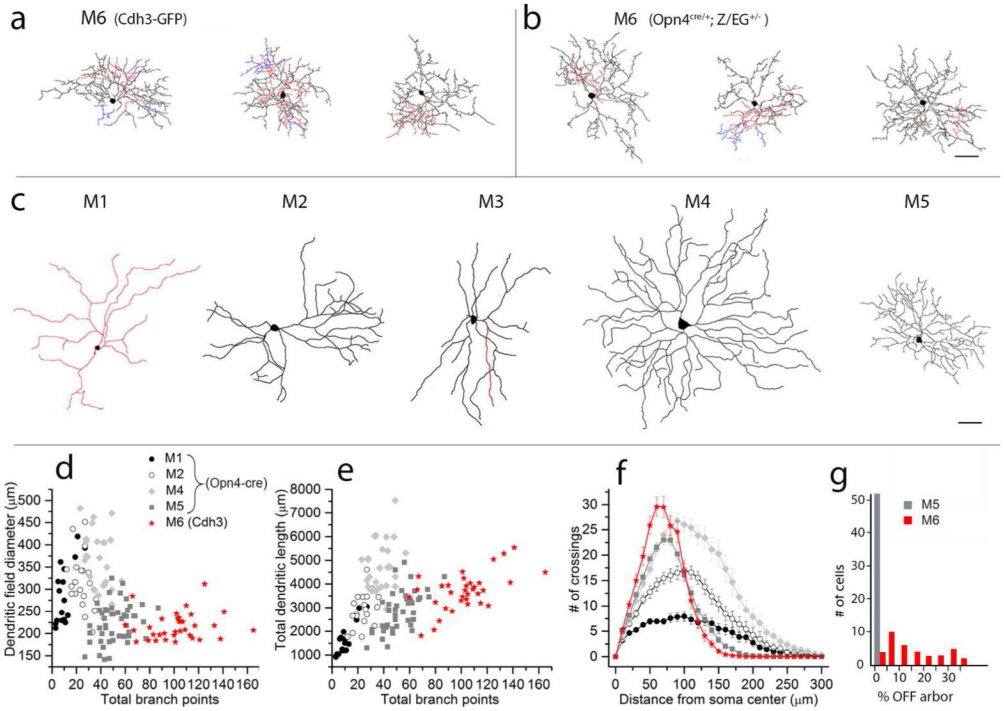

Figure 4.

Morphological comparisons of M6 cells to other ipRGC types based on traced micrographs of dye filled cells. (a, b) Tracings of M6 cells drawn from Cdh3-GFP mice (a) or from Opn4$^{cre/+}$;Z/EG$^{+/-}$ mice (b). c: Tracings of representative M1-M5 cells from Opn4-Cre mice. In a-c, dendrites in the ON sublayer are black, those in the OFF sublayer are red, and those that return to the ON sublayer after diving into the OFF sublayer are blue. Scale bar in (c) equals 50 µm and also applies to (a,b). (d-e) Scatterplots comparing morphological parameters of M1, M2, M4 and M5 ipRGCs from the Opn4$^{cre/+}$;Z/EG$^{+/-}$ mouse line (grey and black symbols) compared to M6 cells from Cdh3-GFP mouse line (red). Total branch points are related to dendritic field diameter (d) or total dendritic length (e) for M1 (n = 17), M2 (n = 20), M4 (n = 27) and M5 (n = 44) cells. Overall, M6 cells have greater total dendritic length than M1 and most M2 cells, and many more branch points than M1, M2, or M4 cells. (f) Sholl analysis comparing dendritic branching patterns for M1 (n = 16), M2 (n = 17), M4 (n = 18) and M5 (n = 44) cells. M6 cells have many more dendritic branches than M1 or M2 cells. Though they have only slightly more dendrites total than M4 cells, these are compressed into a much more compact dendritic arbor. M1, M2, M4 and M5 data were replotted from Estevez et al., 2012 and Stabio et al., 2018. (g) Bar plots showing the variability among M6 cells from Cdh3-GFP (red) in the percentage of total dendritic length found within the OFF sublamina of the IPL; M5 cells (grey), shown for comparison, invariably lack any OFF arbor. Note that the M5 population plotted here consists of 8 monostratified cells from Cdh3-GFP line and 44 M5 cells from the Opn4$^{cre/+}$;Z/EG$^{+/-}$ line replotted from Stabio et al., 2018; all lack an off arbor.

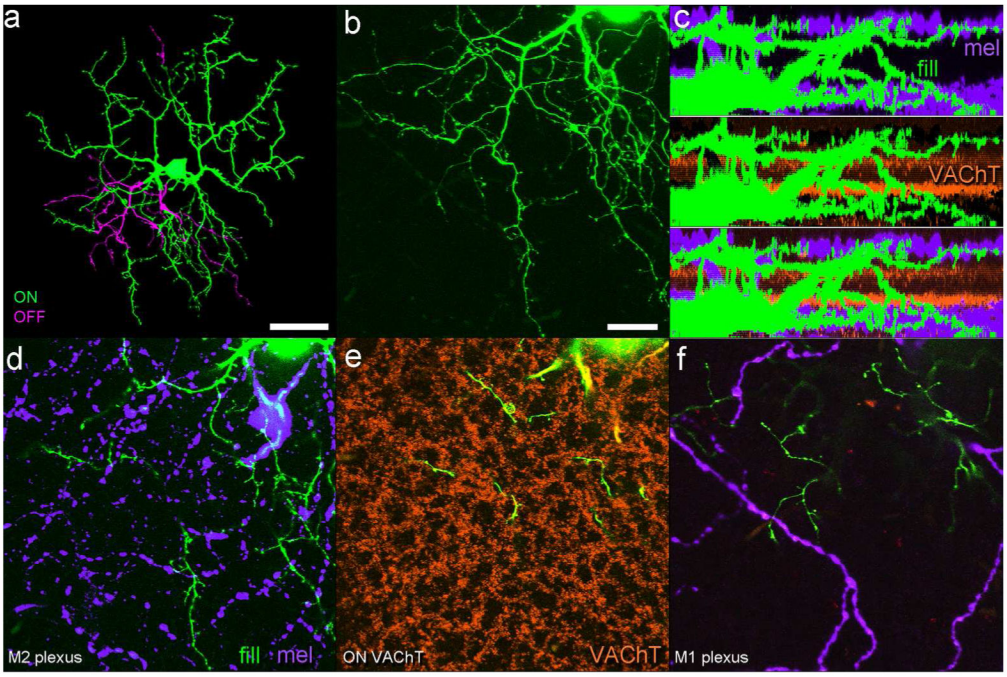

Figure 5.

Dendritic stratification of a representative dye-filled M6 cell (green and magenta) in relation to two sets of laminar benchmarks: the cholinergic bands (marked by anti-VAChT immunostaining in orange); and the dendrites of M1 and M2 ipRGCs (marked by anti-melanopsin immunolabeling in purple). (a) Low-power maximum intensity projection of the cell as viewed *en face*, pseudocolored to differentiate the main inner arbor (green) from the more modest outer arbor (magenta). (b) Higher power view of lower left sector of the arbor, illustrating the fine spines and short branches typical of the M6 type (stratification not color coded as in a). (c) Three matching side-view projections of the entire dendritic arbor of the filled M6 cell (green) in relation to the melanopsin immunopositive dendrites of M1 and M2 ipRGCs (purple; top panel), the VAChT-immunopositive processes of starburst amacrine cells (orange; middle panel), and both laminar markers (bottom panel). Note stratification of dendrites at two distinct levels within the IPL, corresponding to those occupied by dendrites of M1 and M2 ipRGCs. (d-f) Three optical planes through the same region of the arbor shown in (b). (d) View at the level of the main inner arbor of the filled M6 cell, which intermingles with the plexus of M2 ipRGC dendrites (purple). (e) View at the level of the ON cholinergic plexus (orange), where few if any terminal branches are present, though dendritic segments connecting the inner and outer arbors are visible. (f) View at the level of the outer arbor of the filled M6 cell, where they costratify with terminal dendrites of M1 ipRGCs (purple). Scalebars are 50 μm in (a) and 20 μm in (b).

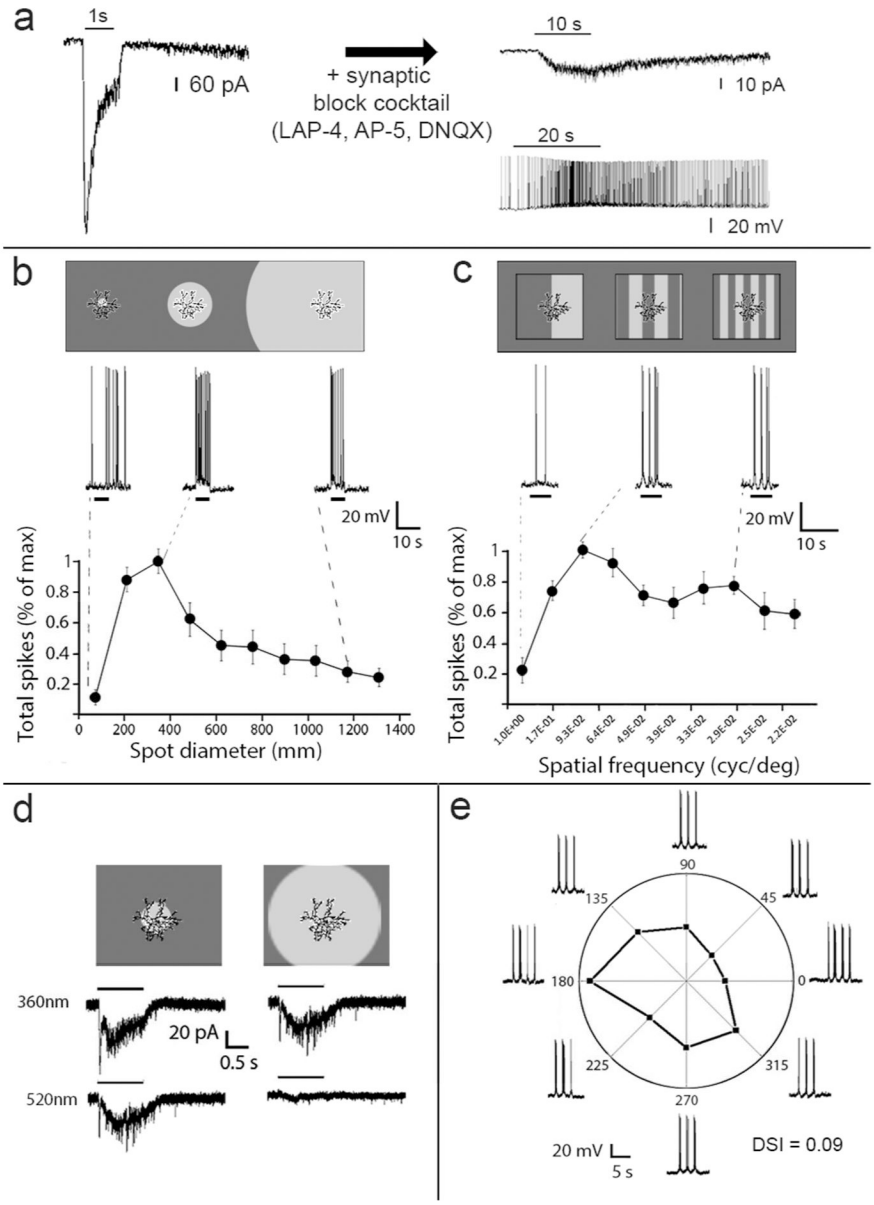

Figure 6.

Light responses of M6 ipRGCs. (a) Photoresponses of M6 cells in normal Ames medium (left) and after pharmacological blockade of chemical synapses (right) reveal both extrinsic and intrinsic photosensitivity, respectively. Intrinsic responses are shown in both voltage clamp (right top) and current clamp (right bottom). (b) Response of M6 cells to flashed spots of varying size (n = 10 M6 cells). Cartoon at top shows spot sizes in relation to the dimensions of the dendritic field. Representative current clamp traces (middle) show depolarization and spiking evoked by the corresponding light spot. Plot at bottom show normalized spike response as a function of spot diameter. Note the strong suppressive effect of stimulation beyond the dendritic field. (c) Tuning of M6 cells (n = 6) to the spatial frequency of drifting sinusoidal gratings (d) Absence of chromatically opponent surround in M6 cell. Surround stimulation with green light (520 nm) attenuates the center response but

never inverts it, as it does in chromatically opponent M5 cells (see Figure 7c). (e) Absence of direction selectivity in a representative M6 cell. Directional selectivity was tested in a total of 6 M6 cells; none showed directional tuning.

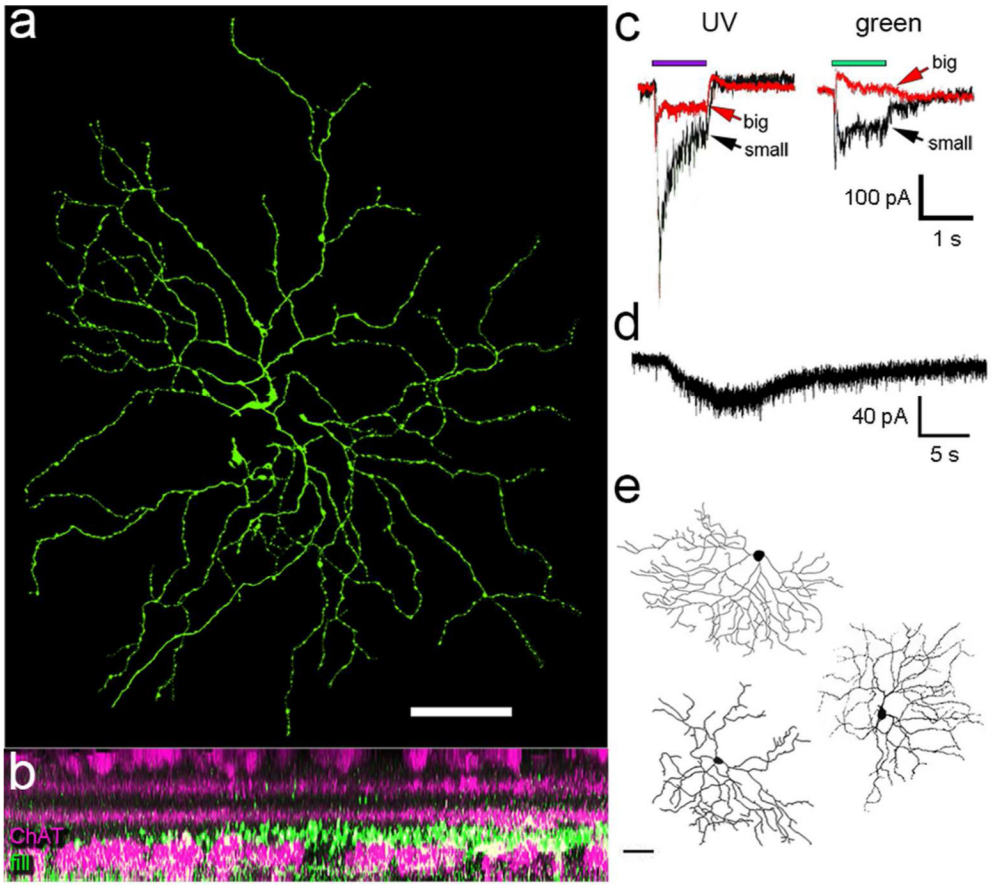

Figure 7.

Chromatically opponent M5 ipRGCs are among the GFP-positive ganglion cells in the Cdh3-GFP mouse. (a-d) An example M5 cell targeted for patch recording and dye filling based on GFP fluorescence in the Cdh3-GFP mouse. (a) Dendritic morphology as viewed *en face*. Maximum intensity projection of the full dendritic arbor, revealed by dye filling. Soma was lost when the patch pipette was withdrawn. (b) Side-view projection of the full dendritic arbor (green) in relation to the ChAT bands (magenta; anti-ChAT immunolabeling). Dendrites stratify exclusively proximal to (below) the ON ChAT band. The confocal z-stack from which this view was generated was first digital flattened to correct for tissue warp. (c) Voltage clamp recordings of this cell's current responses to narrowband spectral stimuli. Note that when stimuli were big (620 μm diameter; red traces), UV stimuli (360 nm) evoked excitatory inward currents, while green stimuli (520 nm) evoked inhibitory outward current. Smaller spots (165 μm; black traces) evoked excitatory currents for either wavelength. This spectral behavior is typical of M5 ipRGCs (Stabio et al., 2018). (d) This cell was intrinsically photosensitive in the presence of LAP-4 which blocks the synaptically driven ON response. A slow inward current was elicited in response to 5 s step of 480 nm light ($3.3 \cdot 10^{16}$ photons·$s^{-1}cm^{-2}$). (e) Tracings of several other monostratified presumptive M5 cells among intracellularly dye-filled GFP-positive cells from Cdh3 mice.

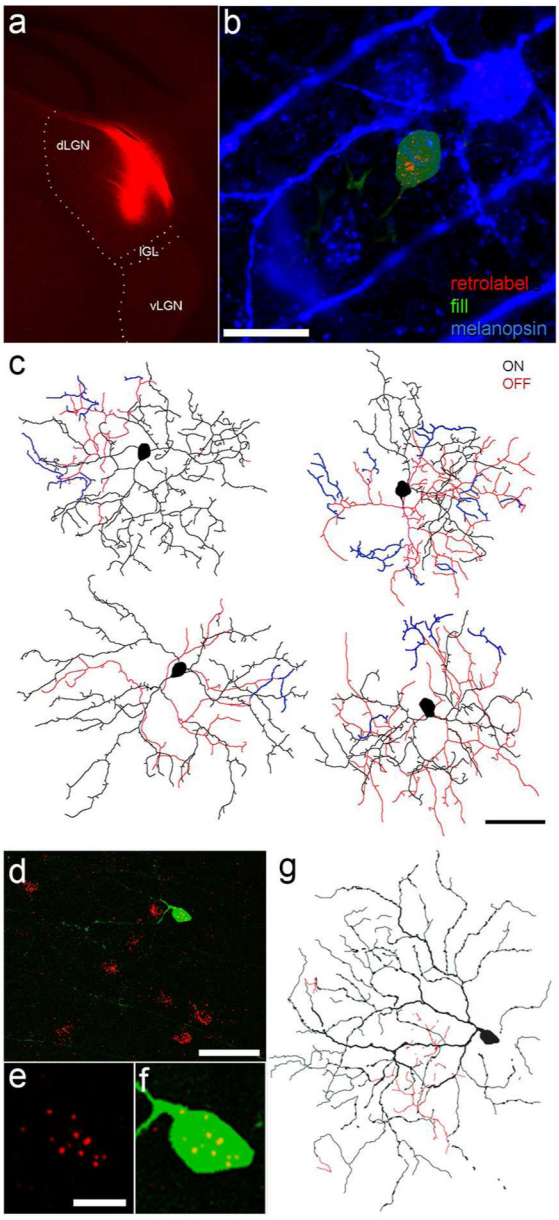

Figure 8.

Evidence that M6 ipRGCs innervate the dorsal lateral geniculate nucleus (dLGN). (a) Deposit of a red fluorescent retrograde tracer (cholera toxin β-subunit conjugated to Alexa Fluor 594) into the right dLGN of a melanopsin reporter mouse. The intergeniculate leaflet (IGL) and ventral lateral geniculate nucleus (vLGN) are spared. (b) Example of a retrolabeled and dye-filled M6 cell in the contralateral retina of this mouse. The cell was targeted for dye filling (green) based on co-labeling by GFP fluorescence (indicating its identity as an ipRGC) and retrolabeling (red), indicating that it innervated the dLGN. The cell is substantially smaller than the adjoining M2 ipRGC, marked by intense melanopsin immunofluorescence (blue). Scale bar: 20 μm. Maximum intensity projection of three serially adjacent optical sections. Bleed-through of fluorescent channels has been digitally

subtracted. (c) Tracing of the somadendritic profile of the cell shown in (b) (upper left tracing) and of three other retrolabeled M6 cells dye-filled in the same retina. Scale bar: 50 μm. (d-g) Confirmatory data from another retina by an alternative method. A Cre-dependent virus injected into the eye of an Opn4-Cre mouse induced GFP expression in fraction of ipRGCs. Subsequent injection of a red latex microspheres into the contralateral dLGN induced retrolabeling of a subset of afferent ganglion cells. One well-isolated double-labeled cell is shown in (d) (scale bar: 50 μm, and at higher magnification in (e) (retrobeads only) and (f) (merged retrobeads and GFP); scale bar: 10 μm. (g) Drawing of the somadendritic profile of this cell, with morphology characteristic of the M6 type (scale and conventions same as for (c)). Injection site for this experiment appears in Figure 6a of Stabio et al., 2018. In panel c and g, dendrites in the ON sublayer are black, those in the OFF sublayer are red, and those that return to the ON sublayer after diving into the OFF are blue.

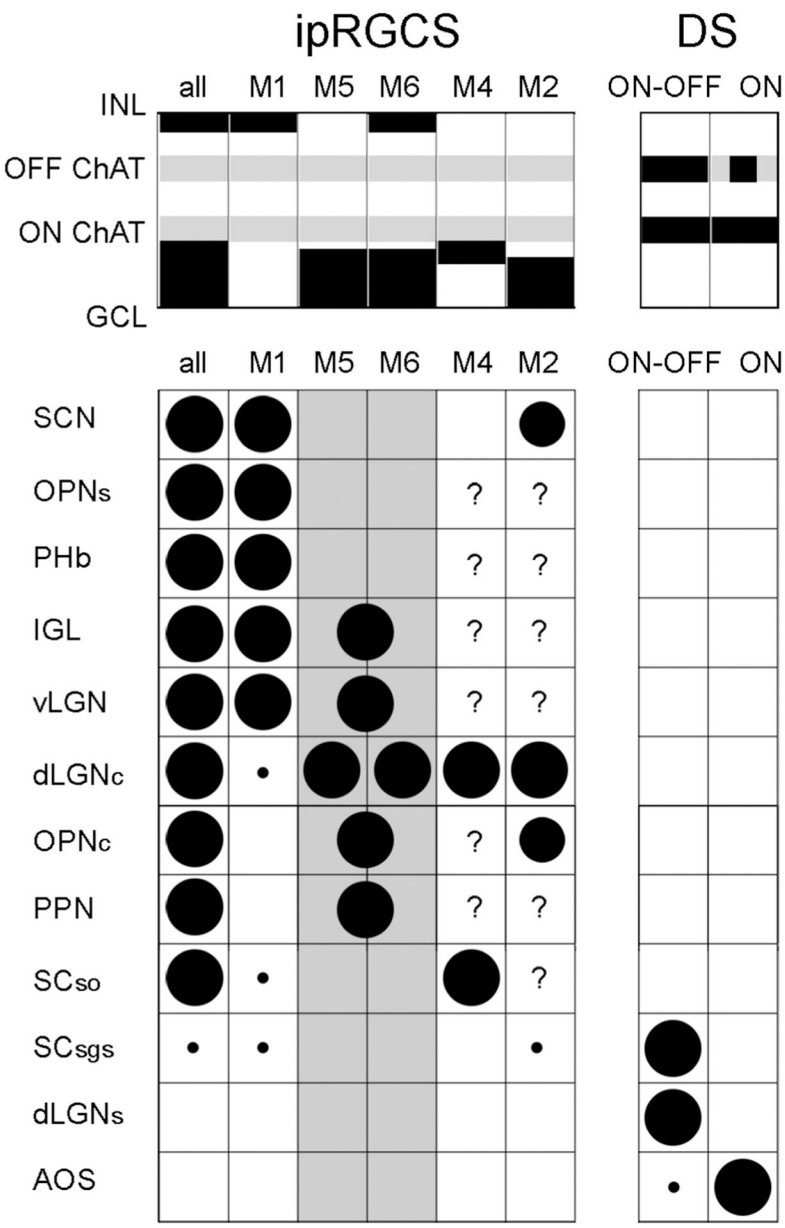

Figure 9.

Tabulation of differences among direction selective (DS) RGCs and major subtypes of ipRGCs (M1-M6) in dendritic stratification and brain targets. In the top schematic, dendritic stratification of each type is indicated by black rectangles. Grey stripes indicate the two cholinergic bands as laminar benchmarks. Dendrites of DS-RGCs are bistratified and stratify selectively in these bands; in ON DS-RGCs, the ON arbor dominates. When considered collectively, ipRGC dendrites are found in two bands, distal to (above) the OFF ChAT band, and proximal (below) the ON ChAT band (left column; “all”). However, individual ipRGC subtypes differ in stratification, with M1 cells stratifying only distal, M2, M4, and M5 cells only proximal, and M6 cells in both sublayers. M3 cells match the stratification of M6 cells,

but are not included because it remains unclear if they comprise a bona fide subtype and almost nothing is known of their brain projections.

The table summarizes current evidence on the *axonal projections of these cell types* to specific retinorecipient nuclei of the midbrain and diencephalon. Circles indicate an established projection; diameter indicates strength. If evidence suggests a projection is lacking, the corresponding cell has been left empty; where no relevant evidence exists, the cell contains a question mark. For M5 and M6 cells (columns shaded grey), projections have been inferred largely form GFP+ optic axons in the Cdh3-GFP mouse. Though these derive mostly from M6 cells, M5 cells also contribute; circles straddle the column boundary between M5 and M6 cells to reflect this ambiguity. The ambiguity is resolved only for the core of the dLGN, where both subtypes have confirmed projections by means of retrograde tracing. Note that M5 and M6 cells project to non-image-forming visual centers that are largely distinct from those innervated by M1 cells and that there is almost no overlap in brain projections between ipRGCs and DS-RGCs. Citations (for projection evidence, along with this manuscript): (Baver, Pickard, Sollars, & Pickard, 2008; Brown et al., 2010; Ecker et al., 2010; Estevez et al., 2012; Hattar et al., 2006; Hattar, Liao, Takao, Berson, & Yau, 2002; Osterhout et al., 2014; Osterhout et al., 2011; Stabio et al., 2018; Zhao et al., 2014). Abbreviations: SCN – suprachiasmatic nucleus; OPNs – shell of the olivary pretectal nucleus; PHb – perihabenular nucleus of the thalamus; IGL - intergeniculate nucleus; vLGN – ventral division of the lateral geniculate nucleus; dLGNc – core of the dorsal division of the LGN; OPNc - core of the olivary pretectal nucleus; PPN - posterior pretectal nucleus; SCso – stratum opticum of the superior colliculus; SCsgs – superficial gray layer of the superior colliculus; dLGNs – shell of the dLGN; AOS - accessory optic system.

Table 1:

Antibodies used in this study

Name	Host	Polyclonal or monoclonal?	Source and catalog # and RRID	Dilution	RRID
ChAT	Goat	Polyclonal	Millipore Cat# AB144P	1:200	RRID: AB_2079751
VAChT	Guinea pig	Polyclonal	Millipore Cat # AB1588	1:1000	RRID: AB_1121411 0
Melanopsin	Rabbit	Polyclonal	Advanced Targeting Systems Cat# AB-N38	1:10,000	RRID: AB_1608077
GFP	Rabbit	Polyclonal	Life Technologies Cat # A-6455	1:1000	RRID: AB_221570
Lucifer Yellow	Rabbit	Polyclonal	Life Technologies Cat # A-5750	1:500	RRID: AB_2536190
Alexa Fluor 350	Donkey anti-goat	Polyclonal	Life Technologies Cat # A-21081	1:200	RRID: AB_2534105
Alexa Fluor 594	Donkey anti-goat	Polyclonal	Life Technologies Cat # A-11058	1:200	RRID: AB_142540
Alexa Fluor 647	Donkey anti-goat	Polyclonal	Life Technologies Cat # A-21447	1:200	RRID: AB_141844
Alexa Fluor 488	Donkey anti-rabbit	Polyclonal	Life Technologies Cat # A-21206	1:200	RRID: AB_2535792
Alexa Fluor 594	Donkey anti-rabbit	Polyclonal	Life Technologies Cat # A-21207	1:200	RRID: AB_141637
Alexa Fluor 488	Goat anti-rabbit	Polyclonal	Life Technologies Cat # A-11008	1:1000	RRID: AB_143165
Alexa Fluor 594	Goat anti-rabbit	Polyclonal	Life Technologies Cat # A-11012	1:1000	RRID: AB_141359
Alexa Fluor 594	Goat anti-guinea pig	Polyclonal	Life Technologies Cat # A-11076	1:1000	RRID: AB_141930
TSA Kit #15, with HRP—Goat Anti-Rabbit IgG and Alexa Fluor 594 Tyramide	Goat anti-rabbit with horseradish peroxidase		Invitrogen Cat# T20925	1:100	RRID: AB_2716806